Edge-Bridging and Face-Capping Coordination of Alkenyl Ligands in Triruthenium Carbonyl Cluster Complexes Derived from Hydrazines: Synthetic, Structural, Theoretical, and Kinetic Studies

Javier A. Cabeza,*[a] Ignacio del Río,[a] José M. Fernández-Colinas,[a] Santiago García-Granda,[b] Lorena Martínez-Méndez,[a] and Enrique Pérez-Carreño[b]

Abstract: The reactions of the triruthenium cluster complex $[Ru_3(\mu\text{-}H)(\mu_3\text{-}\eta^2\text{-}HNNMe_2)(CO)_9]$ (**1**; H_2NNMe_2 = 1,1-dimethylhydrazine) with alkynes (PhC≡CPh, HC≡CH, $MeO_2CC{\equiv}CCO_2Me$, PhC≡CH, $MeO_2CC{\equiv}CH$, $HOMe_2CC{\equiv}CH$, 2-pyC≡CH) give trinuclear complexes containing edge-bridging and/or face-capping alkenyl ligands. Whereas the edge-bridged products are closed triangular species (three Ru–Ru bonds), the face-capped products are open derivatives (two Ru–Ru bonds). For terminal alkynes, products containing *gem* ($RCCH_2$) and/or *trans* (RHCCH) alkenyl ligands have been identified in both edge-bridging and face-capping positions, except for the complex $[Ru_3(\mu_3\text{-}\eta^2\text{-}HNNMe_2)(\mu_3\text{-}\eta^3\text{-}HCCH\text{-}2\text{-}py)(\mu\text{-}CO)(CO)_7]$, which has the two alkenyl H atoms in a *cis* arrangement. Under comparable reaction conditions (1:1 molar ratio, THF at reflux, time required for the consumption of complex **1**), some reactions give a single product, but most give mixtures of isomers (not all the possible ones), which were separated. To determine the effect of the hydrazido ligand, the reactions of $[Ru_3(\mu\text{-}H)(\mu_3\text{-}\eta^2\text{-}MeNNHMe)(CO)_9]$ (**2**; HMeNNHMe = 1,2-dimethylhydrazine) with PhC≡CPh, PhC≡CH, and HC≡CH were also studied. For edge-bridged alkenyl complexes, the Ru–Ru edge that is spanned by the alkenyl ligand depends on the position of the methyl groups on the hydrazido ligand. For face-capped alkenyl complexes, the relative orientation of the hydrazido and alkenyl ligands also depends on the position of the methyl groups on the hydrazido ligand. A kinetic analysis of the reaction of **1** with PhC≡CPh revealed that the reaction follows an associative mechanism, which implies that incorporation of the alkyne in the cluster is rate-limiting and precedes the release of a CO ligand. X-ray diffraction, IR and NMR spectroscopy, and calculations of minimum-energy structures by DFT methods were used to characterize the products. A comparison of the absolute energies of isomeric compounds (obtained by DFT calculations) helped rationalize the experimental results.

Keywords: alkenyl ligands · alkynes · cluster compounds · N ligands · ruthenium

Introduction

Alkenyl groups are important ligands in organometallic chemistry because they are related to many metal-mediated transformations of alkynes and alkenes. However, to date, only a few triruthenium carbonyl cluster complexes containing alkenyl ligands are known,[1–4] despite the fact that some of these clusters have been recognized as intermediates or as catalyst precursors for alkyne–alkene codimerization[5] and alkyne hydrogenation,[6] dimerization,[2b] polymerization,[2b] and hydroformylation[2c] processes.

Most of these alkenyl complexes were prepared by treating hydrido carbonyl cluster complexes with alkynes (by insertion of the alkyne into the M–H bond). When the starting hydrido carbonyl cluster complexes contain a bridging ancillary ligand (this is the most common situation), the shape of this ligand may result in the existence of symmetry-unrelated metal–metal edges, and when these clusters react with alkynes, different isomeric edge-bridged alkenyl derivatives may be formed as a result of the attachment of the alkenyl ligand to metal atoms of different M–M edges. Generally, these reactions are regioselective and only one of

[a] Prof. J. A. Cabeza, Prof. I. del Río, Prof. J. M. Fernández-Colinas, L. Martínez-Méndez
Departamento de Química Orgánica e Inorgánica
Instituto de Química Organometálica "Enrique Moles"
Universidad de Oviedo, 33071 Oviedo (Spain)
Fax: (+34) 985-103-446
E-mail: jac@fq.uniovi.es

[b] Prof. S. García-Granda, Prof. E. Pérez-Carreño
Departamento de Química Física y Analítica
Universidad de Oviedo, 33071 Oviedo (Spain)

Supporting information for this article is available on the WWW under http://www.chemeurj.org/ or from the author.

 DOI: 10.1002/chem.200400517

the possible alkenyl derivatives is formed, but the factors that govern this regioselectivity have not been studied. In this context, while studying the reactivity of diphenylacetylene with hydrido triruthenium clusters that contain face-capping 2-aminopyridine-derived ligands, namely, $[Ru_3(\mu\text{-}H)(\mu_3\text{-}\eta^2\text{-}RNpy)(CO)_9]$ (where HRNpy represents a 2-aminopyridine with R on the amino N atom),[1f,2] we observed that only derivatives with edge-bridging alkenyl ligands have been reported and that the nature of the R group of the ancillary ligand directs the coordination of the alkenyl ligand to the Ru atoms of a particular edge of the metal triangle. Thus, for R = H, both the alkenyl and the amido groups span the same Ru–Ru edge,[1f] whereas for R ≠ H, these groups span different Ru–Ru edges[2] (e.g., the reactions shown in Scheme 1).

About a decade ago, Süss-Fink et al. reported the synthesis of hydrido triruthenium carbonyl cluster complexes containing face-capping ligands derived from hydrazines,[7] $[Ru_3(\mu\text{-}H)(\mu_3\text{-}\eta^2\text{-}R^1NNR^2Me)(CO)_9]$ (Scheme 2), and Hansert and Vahrenkamp studied their reactions with phenyl- and diphenylacetylene.[4] The latter reported a similar behavior for both alkynes, each reaction giving a mixture of three trinuclear alkenyl products (Scheme 2): a closed octacarbonyl complex in which the alkenyl group and the amido fragment of the hydrazido ligand span different Ru–Ru edges (**A**), an open octacarbonyl complex having a face-capping alkenyl ligand (**B**), and a poorly characterized nonacarbonyl derivative (**C**). Changes in the nature of the groups attached to the hydrazine-derived fragment (cluster compounds derived from methylhydrazine, 1,1-dimethylhydrazine, and 1,2-dimethylhydrazine were used) affected the ratio of the product mixtures, but not to the extent of precluding formation of any of the three products.[4]

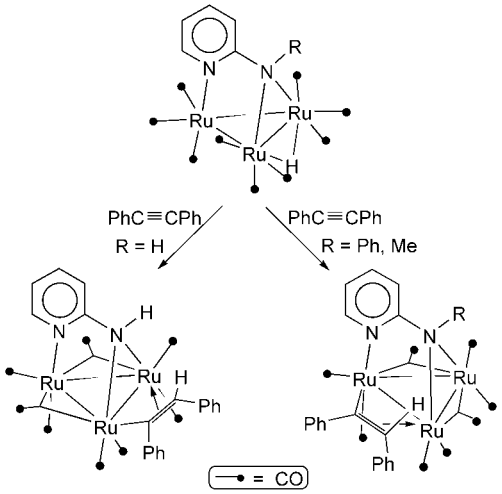

Scheme 1. Reactivity of 2-aminopyridine-derived hydrido triruthenium clusters with alkynes.

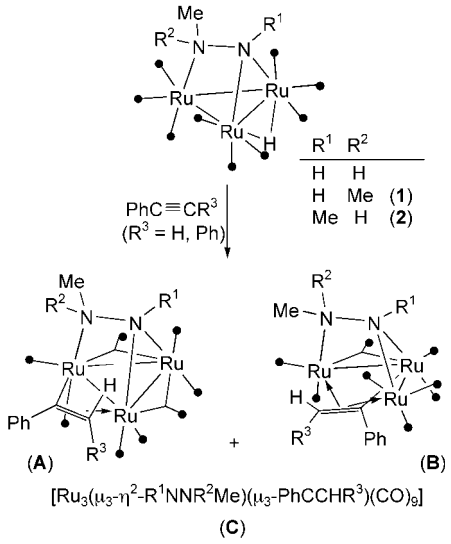

Scheme 2. Reactivity of phenyl- and diphenylacetylene with hydrazine-derived hydrido triruthenium clusters (as reported by Hansert and Vahrenkamp).

We found the results of Hansert and Vahrenkamp intriguing for several reasons. 1) For the edge-bridged compounds **A**, the edge spanned by the alkenyl group is always different from that spanned by the amido fragment, regardless of the nature of the R^1 group. However, this contrasts with our observation that, for 2-aminopyridine-derived clusters, different R groups attached to the N atom of the amido fragment direct the alkenyl ligand to different edges of the metal triangle (Scheme 1). 2) The alkenyl ligands of all the products derived from phenylacetylene have their H atoms in *gem* positions, which implies that only a Markovnikov-type insertion process takes place. However, *trans*-alkenyl ligands are also known in carbonyl cluster chemistry.[8] 3) Trimetallic clusters bearing face-capping alkenyl ligands are very rare, not only for ruthenium, but also for other metals. This type of coordination has been found in $[Os_3(\mu\text{-}H)(\mu_3\text{-}\eta^2\text{-}CF_3CCHCF_3)(CO)_{10}]$,[9] $[WRu_2(\mu\text{-}NPh)(\mu_3\text{-}\eta^2\text{-}CF_3CCHCF_3)(\eta^5\text{-}C_5Me_5)(CO)_7]$,[10] $[Ru_3\{\mu_3\text{-}NS(O)MePh\}(\mu_3\text{-}\eta^2\text{-}RCCHR)(\mu\text{-}CO)(CO)_7]$,[3a] and compounds **B**. 4) According to the EAN rules, saturated trinuclear compounds with two M–M bonds should be 50-electron species.[11] However, compounds **B** are open (two Ru–Ru bonds) 48-electron species.

To shed some light on the questions arising from the aforementioned observations, and being aware of the importance of alkenyl ligands in organometallic chemistry, we decided to reinvestigate the reactivity of alkynes with the Süss-Fink hydrido triruthenium carbonyl clusters derived from hydrazines. We initially studied the reactions of $[Ru_3(\mu\text{-}H)(\mu_3\text{-}\eta^2\text{-}HNNMe_2)(CO)_9]$ (**1**) and $[Ru_3(\mu\text{-}H)(\mu_3\text{-}\eta^2\text{-}MeNNHMe)(CO)_9]$ (**2**) with phenyl- and diphenylacetylene, and while attempting to rationalize the obtained results, which differ considerably from those reported by Hansert and Vahrenkamp,[4] we carried out a deeper study that involved the use of other alkynes. X-ray diffraction, IR and NMR spectroscopy, and calculations of minimum-energy structures by DFT methods were used to characterize the products. A comparison of the absolute energies of isomeric compounds (obtained by DFT calculations) helped rationalize the experimental results. A kinetic analysis of the reaction of **1** with diphenylacetylene is also reported. It sheds some light on the mechanism of these reactions.

Results and Discussion

Reactivity studies: All reactions were carried out in a systematic way with THF as solvent and a 1:1.1 cluster-to-alkyne ratio, except for the reactions with acetylene, which were carried out by bubbling the alkyne through the solution of the corresponding complex. The reaction solutions were stirred at reflux temperature until the complete disappearance of the starting complex (**1** or **2**) was observed by IR spectroscopy and/or spot TLC. All isolated products are collected in Schemes 3 and 4. The results are summarized in Table 1,

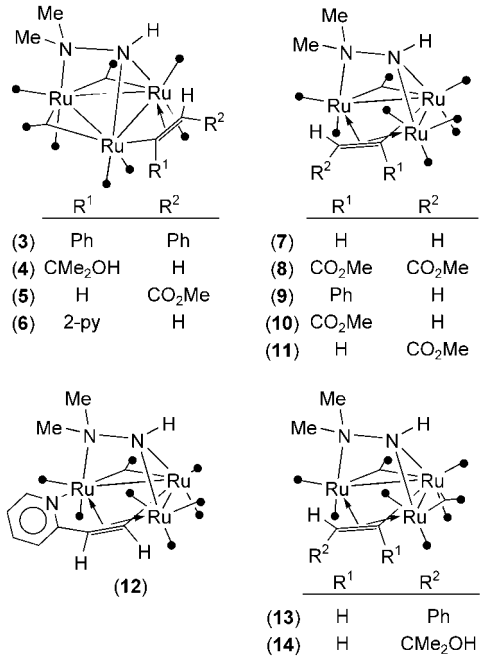

Scheme 3. Numbering scheme for the products isolated from **1**.

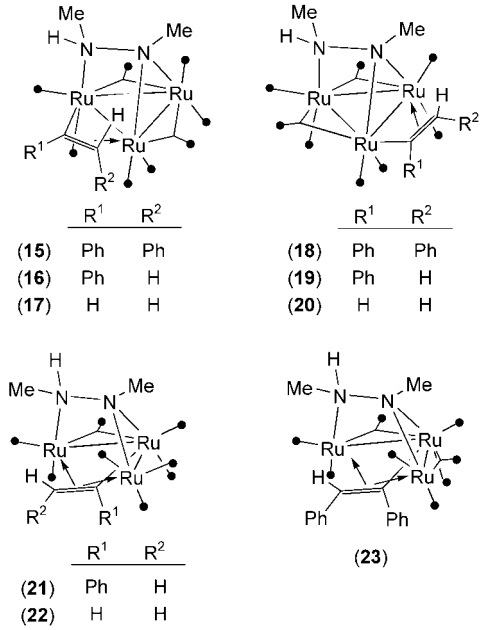

Scheme 4. Numbering scheme for the products isolated from **2**.

Table 1. Reagents and isolated products.

Reagents	Products (color, yield)
1+HC≡CH	**7** (orange, 89%)
1+$MeO_2CC{\equiv}CCO_2Me$	**8** (orange, 47%)
1+PhC≡CPh	**3** (red, 79%)
1+2-pyC≡CH	**6** (orange, 17%), **12** (red, 12%)
1+$HOMe_2CC{\equiv}CH$	**4** (orange, 12%), **14** (yellow, 39%)
1+$MeO_2CC{\equiv}CH$	**5** (orange, 6%), **10** (orange, 43%), **11** (orange, 16%)
1+PhC≡CH	**9** (orange, 57%), **13** (orange, 20%)
2+HC≡CH	**17** (orange, 30%), **20** (orange, 10%), **22** (yellow, 34%)
2+PhC≡CPh	**15** (orange, 23%), **18** (red, 19%), **23** (yellow, 6%)
2+PhC≡CH	**16** (orange, 29%), **19** (red, 18%), **21** (yellow, 27%)

in which the reactions are arranged by alphabetical order of the alkyne used with each starting complex (as in the Experimental Section). Except for the reactions of **1** with acetylene and diphenylacetylene, which gave single products, the remaining reactions gave mixtures of several isomers that were separated by chromatographic methods (mostly TLC). Very weak chromatographic bands were not worked up.

To confirm or reject the possibility that some isomeric products could be intermediates in the formation of other isomers, some representative reactions were carried out. Compounds **5**, **10**, and **11** (all arising from the reaction of **1** with methyl propiolate in refluxing THF, 30 min) were individually heated in refluxing THF. While compounds **5** and **11** remained unaltered, complete transformation of the μ_3-*gem* isomer **10** into the μ_3-*trans* isomer **11** was observed after 2 h. However, this long reaction time contrasts with the short reaction time (30 min) required for the reaction of **1** with methyl propiolate, which also gives a considerable amount of **11**.

Similarly, heating a 3:1 mixture of the μ_3-*gem* and μ_3-*trans* isomers **9** and **13** (i.e., the crude reaction mixture obtained from **1** and phenylacetylene in THF, reflux, 20 min) in toluene at reflux temperature for 10 min, allowed the preparation of pure complex **13**. The latter transformation took 2 h when it was carried out in refluxing THF.

As the *trans* products are formed together with the *gem* products in the reactions of **1** with the appropriate terminal alkynes after short reaction times (and/or at low temperatures) and the observed *gem* to *trans* isomerization processes require longer reaction times (and/or higher temperatures), the *trans* products observed in the reactions of **1** with some terminal alkynes should not arise, at least to a great extent, from the *gem* products (by an isomerization process which has a considerable kinetic barrier). On the contrary, it is reasonable to propose that both the *gem* and *trans* isomers formed from **1** after short reaction times arise from a common early intermediate that evolves through different pathways (Markovnikov and anti-Markovnikov insertion of the alkyne into the Ru–H bond) to give the observed products.

X-ray diffraction studies: The structures of **3**, **5**, **10**, **11**, **12**, and **15** were determined by X-ray diffraction. For compari-

Table 2. Selected interatomic distances [Å] in **3**, **5**, **10**, **11**, **12**, **13**, and **15.**

	3[a]	**5**[a]	**10**[a]	**11**[a]	**12**[a]	**13**[b]	**15**[a]
Ru1–Ru2	2.7031(6)	2.714(1)	2.7714(7)	2.7807(4)	2.804(1)	2.789	2.686(1)
Ru1–Ru3	2.7510(6)	2.755(1)	3.7672(8)	3.7511(4)	3.828(1)	3.896	2.794(1)
Ru2–Ru3	2.7973(6)	2.793(1)	2.7941(7)	2.7818(5)	2.828(1)	2.875	2.781(1)
N1–Ru1	2.139(4)	2.132(8)	2.127(6)	2.134(4)	2.15(1)	2.198	2.155(8)
N1–Ru2	2.133(5)	2.125(8)	2.096(6)	2.099(4)	2.09(1)	2.145	2.115(8)
N2–Ru3	2.196(5)	2.195(8)	2.226(6)	2.202(4)	2.251(9)	2.319	2.147(8)
N3–Ru3					2.16(1)		
C3–Ru1	2.104(5)	2.077(9)	2.223(7)	2.212(4)	2.30(1)	2.311	2.24(1)
C3–Ru2	2.235(5)	2.159(9)	2.223(7)	2.127(4)	2.33(1)	2.267	
C3–Ru3			2.257(7)	2.274(4)	2.21(1)	2.325	2.13(1)
C4–Ru1			2.216(8)	2.225(4)	2.23(1)	2.539	2.29(1)
C4–Ru2	2.271(5)	2.265(9)					
C4–Ru3			2.533(8)	2.512(4)	2.65(1)	2.539	
C3–C4	1.406(8)	1.36(1)	1.44(1)	1.444(6)	1.48(2)	1.403	1.42(1)
C10–Ru1	2.007(6)	2.007(9)					
C10–Ru3	2.558(6)	2.65(1)					
C11–Ru1			1.93(1)	1.92(1)	1.98(1)	2.018	2.15(1)
C11–Ru2			2.96(1)	3.08(1)	2.85(1)	2.249	1.95(1)
C20–Ru2	2.249(6)	2.16(1)	2.066(7)	2.044(4)	1.98(1)	2.187	2.69(1)
C20–Ru3	1.977(7)	1.96(1)	2.048(7)	2.069(4)	2.05(1)	2.043	2.01(1)

[a] X-ray diffraction data. [b] Calculated by DFT methods (structure **XV**).

son purposes, a common atom numbering scheme was used as far as possible for all structures. Selected interatomic distances are given in Table 2.

The structures of **3** and **5** (Figure 1) correspond to complexes containing edge-bridging alkenyl ligands derived from reactions of **1** with diphenylacetylene (**3**) and methyl propiolate (**5**), respectively. The latter is an example of a *trans* arrangement of two H atoms on an edge-bridging alkenyl group. In both cases, these ligands span the same Ru–Ru edge as the amido fragment of the hydrazido group and are attached to Ru1 through C3, and to Ru2 through C3 and C4, in an analogous manner to that found previously for other edge-bridging alkenyl ligands.[1–3] Both compounds have eight CO ligands, six of which are terminal, one is bridging (in a somewhat asymmetric fashion, since the C20–Ru2 and C20–Ru3 distances differ by ca. 0.2 Å), and one is semibridging (the C10–Ru1 distance is ca. 0.6 Å shorter than the C10–Ru3 distance). Both compounds are closed triangular species in which the Ru1–Ru2 edge is 0.05–0.08 Å shorter than the other two edges. The Ru–Ru distances, ranging from 2.71 to 2.78 Å, confirm the presence of Ru–Ru single bonds.[12]

The structures of **10** and **11** (Figure 2) correspond to complexes containing face-capping alkenyl ligands derived from methyl propiolate and **1**. The two molecular structures are

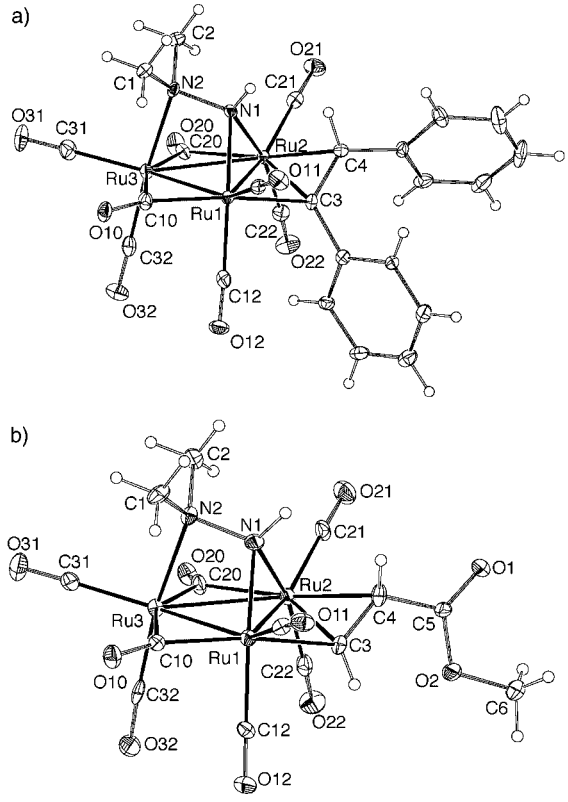

Figure 1. X-ray structures of a) **3** and b) **5**.

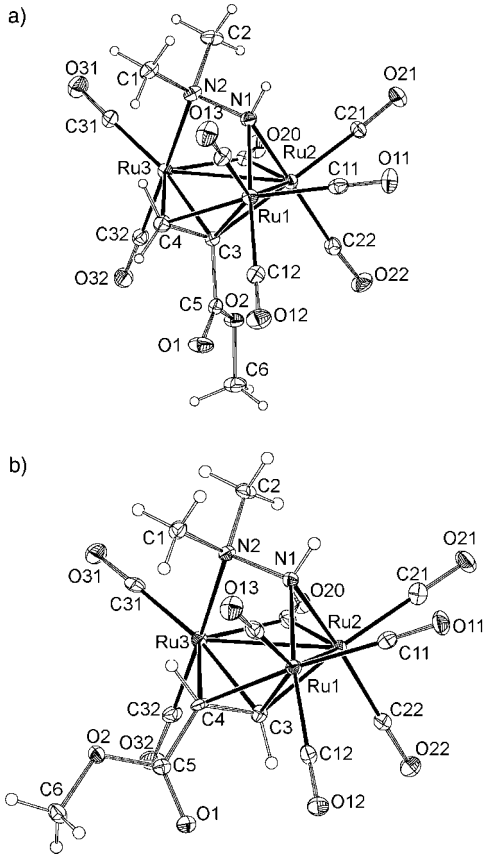

Figure 2. X-ray structures of a) **10** and b) **11**.

nearly identical, except for the arrangement of the substituents of the alkenyl groups. The alkenyl H atoms occupy *gem* positions in **10,** and *trans* positions in **11**. In both cases, the alkenyl ligand is attached to Ru2 through C3 and to Ru1 and Ru3 through C3 and C4, in such a way that the C4–Ru3 distance is about 0.3 Å longer than the others. Both compounds have seven terminal and one bridging CO ligands. They are open triangular species because the lengths of the Ru1–Ru3 edges (3.7672(8) Å in **10** and 3.7511(4) Å in **11**) are outside the bonding range for Ru–Ru bonds.[12] The remaining Ru–Ru distances are in the range 2.77–2.79 Å.

The molecular structure of **12** is shown in Figure 3. This complex, which is derived from the reaction of **1** with 2-ethynylpyridine, contains a face-capping alkenyl ligand with

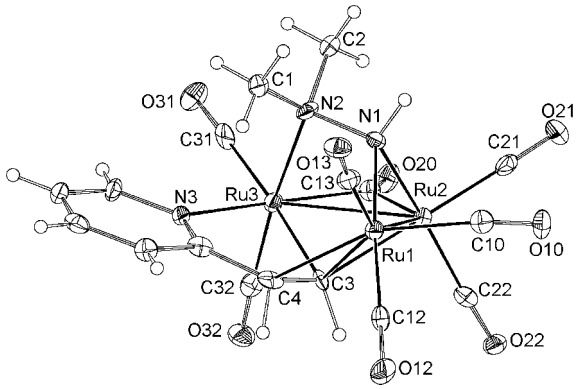

Figure 3. X-ray structure of **12**.

the H atoms in mutual *cis* positions. Such an arrangement must be a consequence of the coordination of the pyridyl N atom to Ru3, which also provokes a lengthening of the C4–Ru3 distance to 2.65(1) Å. All remaining structural features of this compound are comparable with those of **10** and **11**.

The structure of **15** (Figure 4) corresponds to an edge-bridging alkenyl complex derived from the reaction of **2** with diphenylacetylene. In this case, the alkenyl ligand spans the Ru–Ru edge that is close to the hydrogen atom of the 1,2-dimethylhydrazido group and is attached to Ru3 through C3 and to Ru1 through C3 and C4. As in the edge-bridged compounds **3** and **5**, the bridging CO ligand that is *trans* to the alkenyl C3–C4 fragment is slightly asymmetric (C11–Ru1 and C11–Ru2 differ by ca. 0.2 Å), whereas the CO ligand that is *trans* to the σ interaction between the alkenyl ligand and the triruthenium framework, that is, the C3–Ru3 bond, is semibridging (difference between C20–Ru3 and C20–Ru2 is 0.68 Å). As in **3** and **5**, the amido-bridged edge of the metal triangle, Ru1–Ru2, is slightly shorter (by ca. 0.1 Å) than the other two.

Hansert and Vahrenkamp[4] reported the X-ray structures of **9** and **16**. The structure of **9** is comparable to that of **10**, except for the R substituent of the alkenyl fragment. In **16** the alkenyl ligand has a *gem* arrangement of its H atoms and it bridges the Ru–Ru edge adjacent to the NH fragment of the 1,2-dimethylhydrazido ligand, as in **15**.

Intriguingly, despite being 48-electron species, the face-capped alkenyl complexes have only two metal–metal bonds and thus disobey the EAN rules. As noted above, trimetallic clusters bearing face-capping alkenyl ligands are very rare. While $[Os_3(\mu\text{-}H)(\mu_3\text{-}\eta^2\text{-}CF_3CCHCF_3)(CO)_{10}]$[9] and $[WRu_2(\mu\text{-}NPh)(\mu_3\text{-}\eta^2\text{-}CF_3CCHCF_3)(\eta^5\text{-}C_5Me_5)(CO)_7]$[10] are closed 48-electron triangular clusters, Süss-Fink's complexes $[Ru_3\{\mu_3\text{-}NS(O)MePh\}(\mu_3\text{-}\eta^2\text{-}RCCHR)(\mu\text{-}CO)(CO)_7]$[3a] are open (two Ru–Ru bonds) 48-electron triangular clusters.

The alkenyl C3–C4 distances of the face-capped complexes are similar to those of the edge-bridged clusters. This implies that the bond order of the alkenyl C–C bond is similar for both types of complexes. This supports the proposal that the alkenyl ligands behave as three-electron donors in both edge-bridging and face-capping coordination modes. Therefore, all the alkenyl clusters reported in this article are 48-electron species.

IR spectroscopy: Three types of absorption patterns were observed in the carbonyl bond-stretching region of the IR spectra of all these alkenyl complexes (Figure 5). This led us to classify the compounds into three groups (Tables 3–5). Once the structures of one or several members of each group were ascertained by other structural techniques (e.g., NMR spectroscopy, X-ray diffraction, or minimum-energy

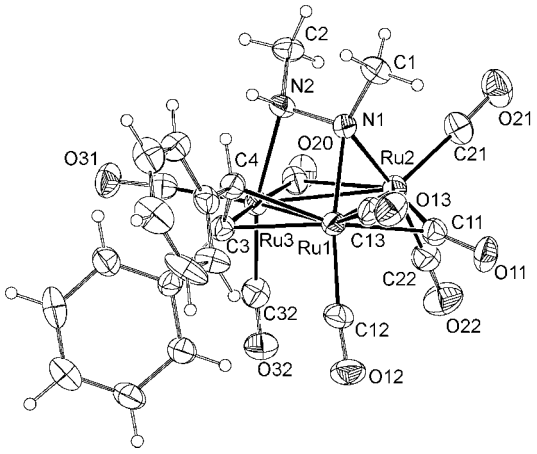

Figure 4. X-ray structure of **15**.

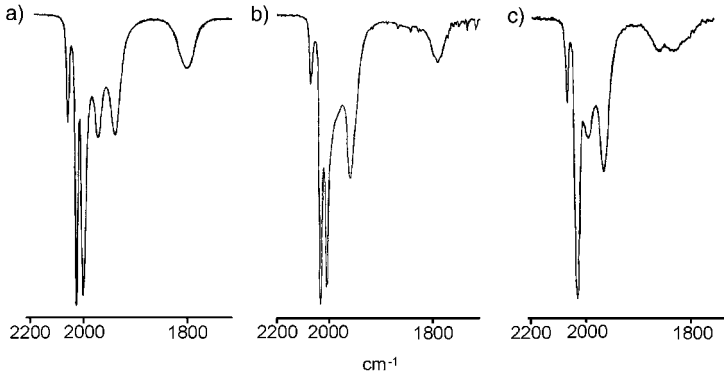

Figure 5. IR spectra of a) **15**, b) **9**, and c) **13** in the ν_{CO} region, as representative examples of the band patterns observed for compounds having an edge-bridging alkenyl ligand (left), a face-capping alkenyl ligand and one bridging CO ligand (center), and a face-capping alkenyl ligand and two bridging CO ligands (right).

Table 3. IR data for the compounds having edge-bridging alkenyl ligands.

Compound	Alkenyl ligand	ν_{CO} (CH_2Cl_2, cm^{-1})
3	PhC=CHPh	2062 (w), 2032 (s), 2011 (s), 1996 (m, sh), 1977 (m), 1949 (m), 1922 (w, sh), 1802 (w, br)
4	$HOMe_2CC=CH_2$	2062 (w), 2030 (s), 2009 (s), 1996 (m, sh), 1973 (m), 1947 (m), 1919 (w, sh), 1803 (m, br)
5	$HC=CHCO_2Me$	2074 (w), 2043 (s), 2017 (s), 1994 (m, sh), 1977 (w, sh), 1956 (m), 1806 (w, br)
6	2-pyC=CH_2	2064 (w), 2034 (s), 2009 (s), 1997 (m sh), 1983 (m), 1944 (m), 1798 (w, br)
15	PhC=CHPh	2068 (w), 2033 (s), 2006 (s), 1974 (m), 1942 (m), 1805 (w, br)
16	PhC=CH_2	2069 (w), 2033 (s), 2006 (s), 1978 (m), 1944 (m), 1806 (w, br)
17	HC=CH_2	2073 (w), 2035 (s), 2003 (s), 1977 (m), 1936 (m), 1804 (w, br)
18	PhC=CHPh	2064 (w), 2032 (s), 2008 (s), 1977 (m), 1950 (m), 1792 (w, br)
19	PhC=CH_2	2064 (w), 2033 (s), 2007 (s), 1979 (m), 1949 (m), 1797 (w, br)
20	HC=CH_2	2069 (w), 2035 (s), 2008 (s), 1979 (m), 1948 (m), 1793 (w, br)

Table 4. IR data for the compounds having one face-capping alkenyl ligand and one bridging CO ligand.

Compound	Alkenyl ligand	ν_{CO} (CH_2Cl_2, cm^{-1})
7	HC=CH_2	2070 (w), 2030 (s), 2009 (s), 1986 (m, sh), 1959 (m), 1792 (w, br)
8	$MeO_2CC=CHCO_2Me$	2085 (w), 2047 (s), 2023 (s), 1999, (w, sh), 1973 (m), 1802 (w, br)
9	PhC=CH_2	2070 (w), 2032 (s), 2010 (s), 1984 (m, sh), 1960 (m), 1792 (w, br)
10	$MeO_2CC=CH_2$	2078 (w), 2040 (s), 2016 (s), 1988 (w, sh), 1966 (m), 1802 (w, br)
11	$HC=CHCO_2Me$	2078 (w), 2040 (s), 2016 (s), 1987 (w, sh), 1968 (m), 1797 (w, br)
12	HC=CH-2-py	2058 (w), 2032 (s), 1999 (m), 1978 (m), 1929 (w), 1739 (w, br)
21	PhC=CH_2	2067 (w), 2033 (s), 2011 (s), 1962 (m), 1792 (w, br)
22	HC=CH_2	2067 (w), 2028 (s), 2009 (s), 1980 (m, sh), 1960 (m), 1804 (w, br)

Table 5. IR data for the compounds having one face-capping alkenyl ligand and two bridging CO ligands.

Compound	Alkenyl ligand	ν_{CO} (CH_2Cl_2, cm^{-1})
13	HC=CHPh	2060 (w), 2021 (vs), 1989 (m), 1959 (m), 1854 (w, br), 1826 (w, br)
14	$HC=CHCMe_2OH$	2062 (w), 2026 (vs), 2008 (s, sh), 1992 (m, sh), 1957 (m), 1840 (w, br), 1821 (w, br)
23	PhC=CHPh	2060 (w), 2019 (vs), 1993 (m), 1958 (m), 1844 (w, br), 1799 (w, br)

DFT calculations), the three groups were identified as being composed of 1) complexes having an edge-bridging alkenyl ligand (Table 3, left spectrum of Figure 5), 2) complexes having a face-capping alkenyl and one bridging CO ligand (Table 4, central spectrum of Figure 5), and 3) complexes having a face-capping alkenyl and two bridging CO ligands (Table 5, right spectrum of Figure 5). Within each group, changes in the nature of the alkenyl ligand substituents affect the position (wavenumber) of the ν_{CO} bands, but they do not significantly alter the relative intensity (transmittance) of the absorptions (the band pattern is maintained). Curiously, all isolated compounds having an edge-bridging alkenyl ligand show the same pattern of ν_{CO} absorptions, regardless of the edge that is spanned by the alkenyl ligand with respect to the face-capping hydrazido fragment. In addition, the ν_{CO} absorptions are also nearly unaffected by the position of the methyl groups on the hydrazido fragment and by the *gem*, *cis*, or *trans* stereochemistry of the alkenyl ligand (maintaining the nature of the substituents).

NMR spectroscopy: Table 6 collects the ^{1}H NMR data of **3**–**23**. All products contain at least one hydrogen atom on the alkenyl ligand, that is, that arising from the original hydrido ligand of starting complex **1** or **2**. The resonance of this proton, which is always *cis* to the Ru atom that is σ-bonded to the alkenyl ligand (except in **12**), is observed in the range $\delta = 2.1$–4.5 ppm. An additional resonance is observed for alkenyl ligands derived from terminal alkynes (excluding acetylene), whose chemical shift and coupling constant depend upon the stereochemistry of the alkenyl ligand. Thus, for *gem*-alkenyls (H atoms in *gem* positions, i.e., **4**, **6**, **9**, **10**, **16**, **19**, and **21**), this resonance always appears at a lower chemical shift (in the range $\delta = 2.8$–1.7 ppm), with a small coupling constant (J in the range 5.6–2.5 Hz), whereas for *trans*-alkenyls (H atoms in *trans* arrangement, i.e., **5**, **11**, **13,** and **14**), it is observed at a high chemical shift (in the range $\delta =$ 10.9–6.4 ppm) with a larger coupling constant (J in the range 14.8–11.9 Hz). The spectrum of **12**, the only complex having a *cis* arrangement of the two hydrogen atoms on the alkenyl ligand, shows two doublets for these protons at $\delta =$ 7.16 and 5.63 ppm, with $J = 7.9$ Hz. The three coupling types (*gem*, *trans*, and *cis*) are observed in the spectra of the products derived from acetylene (**7**, **17**, **20**, and **22**).

Simple ^{1}H NMR spectroscopy was useful for assigning the stereochemistry of the alkenyl ligands in the complexes, but it gave no hint to how the alkenyl ligands are attached to the hydrazido–trimetal framework. Such information was obtained from difference ^{1}H NOE NMR spectra, which helped determine the relative positions of the hydrazido and alkenyl ligands on the clusters. Only two representative examples are presented and discussed here. Difference ^{1}H NOE NMR spectra for **4**, **7**, **15**, **16**, **17**, **19**, **20**, **22**, and **23** are available as Supporting Information.

Figure 6 shows the ^{1}H NMR spectra of **18** (for which IR spectroscopy confirmed the presence of an edge-bridging alkenyl ligand) and the NOE enhancements produced after presaturation at the frequencies of some of its signals. Interestingly, presaturation of the alkenyl CH resonance produced a positive enhancement of the methyl resonance of the bridgehead NMe fragment (trace b) and vice versa (trace d), as expected for protons that are close to each other.[13] Presaturation of the doublet corresponding to the methyl protons of the MeNH group (trace e) or of the quartet of the NH proton (trace c) produced no enhancement of

Table 6. ^{1}H NMR data of compounds **3**–**23**.

Compound	Hydrazido Ligand	Alkenyl Ligand	δ ($CDCl_3$, 20 °C)
3	$HNNMe_2$	PhC=CHPh	7.12 (m, 10H; 2Ph), 3.61 (s, 1H; CH), 3.28 (s, 1H; NH), 2.87 (s, 3H; CH_3), 2.68 (s, 3H; CH_3)
4	$HNNMe_2$	$HOMe_2CC{=}CH_2$	3.68 (d, J=3.1 Hz; CH*H*), 2.82 (brs, 1H; NH), 2.76 (s, 3H; CH_3), 2.61 (s, 3H; CH_3), 1.74 (brs, 1H; OH), 1.68 (s, 3H; CH_3), 1.52 (d, J=3.1 Hz; C*H*H), 1.30 (s, 3H; CH_3)
5	$HNNMe_2$	$HC{=}CHCO_2Me$	10.90 (d, J=11.9 Hz; 1H; CH), 3.75 (s, 3H; CH_3), 2.97 (d, J=11.9 Hz; 1H; CH), 2.76 (s, 3H; CH_3), 2.59 (s, 3H; CH_3), 1.17 (brs, 1H; NH)
6	$HNNMe_2$	2-pyC=CH_2	8.48 (d, br, J=4.4 Hz; 1H; py), 7.64 (td, J=7.6, 1.5 Hz; 1H; py), 7.28 (d, J=7.6 Hz; 1H; py), 7.14 (dd, J=7.6, 4.4 Hz; 1H; py), 3.83 (d, J=2.5 Hz; 1H; CH*H*), 3.16 (brs, 1H; NH), 2.77 (s, 3H; CH_3), 2.62 (s, 3H; CH_3), 2.10 (d, J=2.5 Hz; 1H; C*H*H)
7	$HNNMe_2$	$HC{=}CH_2$	6.43 (dd, J=13.8, 9.8 Hz; 1H; CH), 3.39 (dd, J=9.8, 4.9 Hz; 1H; CH*H*), 2.64 (s, 3H; CH_3), 2.13 (dd, J=13.8, 4.9 Hz; 1H; C*H*H), 2.04 (s, 3H; CH_3) 2.03 (s, 1H; NH)
8	$HNNMe_2$	$MeO_2CC{=}CHCO_2Me$	3.82 (s, 3H; CH_3), 3.56 (s, 3H; CH_3), 2.70 (s, 3H; CH_3), 2.16 (s, 1H; CH), 2.12 (s, 3H; CH_3), 1.82 (s, 1H; NH)
9	$HNNMe_2$	PhC=CH_2	7.10 (m, 3H; Ph), 6.59 (m, 2H; Ph), 3.38 (d, J=5.4; 1H; CH*H*), 2.71 (s, 3H; CH_3), 2.17 (s, 3H; CH_3), 2.16 (s, 1H; NH), 1.70 (d, J=5.4 Hz; 1H; C*H*H)
10	$HNNMe_2$	$MeO_2CC{=}CH_2$	3.52 (s, 3H; CH_3), 3.33 (d, J=5.6 Hz; 1H; CH*H*), 2.64 (s, 3H; CH_3), 2.01 (s, 3H; CH_3), 1.99 (brs, 1H; NH), 1.31 (d, J=5.6 Hz; 1H; C*H*H)
11	$HNNMe_2$	$HC{=}CHCO_2Me$	7.12 (d, J= 12.2 Hz; 1H; CH), 2.82 (d, J=12.2 Hz; 1H; CH), 2.69 (s, 3H; CH_3), 2.36 (brs, 1H; NH), 2.17 (s, 3H; CH_3), 2.11 (s, 3H; CH_3).
12	$HNNMe_2$	HC=CH-2-py	8.05 (d, J=6.7 Hz; 1H; py), 7.81 (d, J=7.9 Hz; 1H; py), 7.67 (dd, J=7.9, 7.3; 1H; py), 7.16 (d, J=9.8 Hz; 1H; CH), 7.03 (dd, J=7.3, 6.7 Hz; 1H; py), 5.63 (d, J=9.8 Hz; 1H; CH), 3.43 (s, 1H; NH), 3.10 (s, 3H; CH_3), 1.32 (s, 3H; CH_3)
13	$HNNMe_2$	HC=CHPh	755 (m, 2H; Ph), 7.31 (m, 3H; Ph), 6.41 (d, J=14.8 Hz; 1H; CH), 4.85 (d, J=14.8 Hz; 1H; CH), 2.71 (s, 3H; CH_3), 2.32 (s, 3H; CH_3), 1.97 (s, 1H; NH)
14	$HNNMe_2$	$HC{=}CHCMe_2OH$	6.60 (d, J=13.6 Hz; 1H; CH), 3.58 (d, J=13.6 Hz; 1H; CH), 2.65 (s, 3H; CH_3), 2.13 (s, 3H; CH_3), 1.94 (s, 1H; NH), 1.75 (s, 3H; CH_3), 1.69 (s, 3H; CH_3), 1.57 (s, 1H; OH)
15	MeNNHMe	PhC=CHPh	7.1 (m, 10H; 2 Ph), 4.83 (s, 1H; *CH*), 3.16 (brq, J=5.5 Hz; 1H; NH), 2.82 (s, 3H; CH_3), 2.73 (d, J=5.5 Hz; 3H; CH_3)
16	MeNNHMe	PhC=CH_2	7.29 (m, 5H; Ph) 4.41 (d, J=4.3 Hz; 1H; CH*H*), 3.40 (d, J=4.3 Hz; 1H; C*H*H), 2.83 (brq, J=5.5 Hz; 1H; NH), 2.72 (s, 3H; CH_3), 2.65 (d, J=5.5 Hz; 3H; CH_3)
17	MeNNHMe	$HC{=}CH_2$	9.87 (dd, J=15.0, 9.9 Hz; 1H; CH), 4.53 (dd, J=9.9, 2.5 Hz; 1H; CH*H*), 3.33 (dd, J=15.0, 2.5 Hz; 1H; C*H*H), 2.86 (brq, J=5.9 Hz; 1H; NH); 2.68 (s, 3H; CH_3), 2.57 (d, J=5.9; 3H; CH_3)
18	MeNNHMe	PhC=CHPh	7.0 (m, 10H; 2 Ph), 4.79 (s, 1H; CH), 3.95 (brq, J=5.5 Hz; 1H; NH), 2.90 (s, 3H; CH_3), 2.76 (d, J=5.5 Hz; 3H; CH_3)
19	MeNNHMe	PhC=CH_2	7.31 (m, 5H; Ph), 3.90 (brq, J=5.9 Hz; 1H; NH), 3.48 (d, J=2.8 Hz; 1H; CH*H*), 3.11 (d, J=2.8 Hz; 1H; C*H*H), 2.73 (d, J=5.9 Hz; 3H; CH_3), 2.67 (s, 3H; CH_3)
20	MeNNHMe	$HC{=}CH_2$	10.55 (dd, J=13.8, 9.8 Hz; 1H; CH), 3.82 (brq, J=5.9 Hz; 1H; NH); 3.67 (dd, J=9.8, 2.4 Hz; 1H; CH*H*), 3.27 (dd, J=13.8, 4.4 Hz; 1H; C*H*H), 2.93 (d, J=5.9 Hz; 3H; CH_3), 2.59 (s, 3H; CH_3)
21	MeNNHMe	PhC=CH_2	7.06 (m, 3H; Ph), 6.92 (m, 2H; Ph), 3.54 (brq, J=5.9 Hz; 1H; NH), 3.33 (d, J=5.1 Hz; 1H; CH*H*), 2.76 (s, 3H; CH_3), 2.13 (d, J=5.9 Hz; 3H; CH_3), 1.58 (d, J=5.1 Hz; 1H; C*H*H).
22	MeNNHMe	$HC{=}CH_2$	6.39 (dd, J=13.5, 9.6 Hz; 1H; CH), 3.43 (dd, J=9.6, 4.4 Hz; 1H; CH*H*), 3.19 (brq, J=5.9 Hz; 1H; NH), 2.65 (s, 3H; CH_3), 2.04 (d, J=5.9 Hz; 3H; CH_3), 2.02 (dd, J=13.5, 4.4 Hz; 1H; C*H*H)
23	MeNNHMe	PhC=CHPh	7.0 (m, 10H; 2Ph), 4.03 (s, 1H; CH), 3.65 (brq, J=5.9 Hz; 1H; N*H*), 2.78 (s, 3H; CH_3), 2.73 (d, J=5.9 Hz; 3H; CH_3)

the alkenyl CH resonance; this confirms that the alkenyl ligand is remote from all H atoms of the MeNH group. The analogous situation observed in the spectra of **19** and **20** (Supporting Information) confirms that they have a similar arrangement of ligands. However, for **15**–**17**, the structures of which have been determined by X-ray diffraction, a positive NOE is observed between the alkenyl CH and the NH resonances (presaturation of one enhances the other), but not between the resonances of any of the methyl groups and the alkenyl CH group (Supporting Information). These data strongly support the structures proposed for these complexes in Scheme 4.

Figure 7 shows the ^{1}H NMR spectrum of compound **21** (for which IR spectroscopy confirmed that it has a face-capping alkenyl ligand) and the NOE enhancements produced after presaturation at the frequencies of some of its signals. Traces (e) and (f) are of particular interest because they unequivocally indicate that the open Ru–Ru edge of the cluster is adjacent to the methyl group of the MeNH moiety. As expected for such a structure, presaturation of the MeNH methyl resonance enhanced one of the alkenyl CH resonances (trace e) and vice versa (trace f). The analogous situation observed in the spectra of **22** and **23** (Supporting Information), confirms that they have a similar ligand arrangement.

Theoretical calculations: Minimum-energy structure calculations were carried out by using DFT methods. Calculations were performed on selected real molecules (products that were isolated in the present work) and on hypothetical ones with the aim of not only comparing the thermodynamic stabilities of real and hypothetical isomeric compounds (important for rationalizing the experimental results), but also to assign or confirm the structures of compounds for which no X-ray diffraction data were available. No simplified model compounds were used for the calculations.

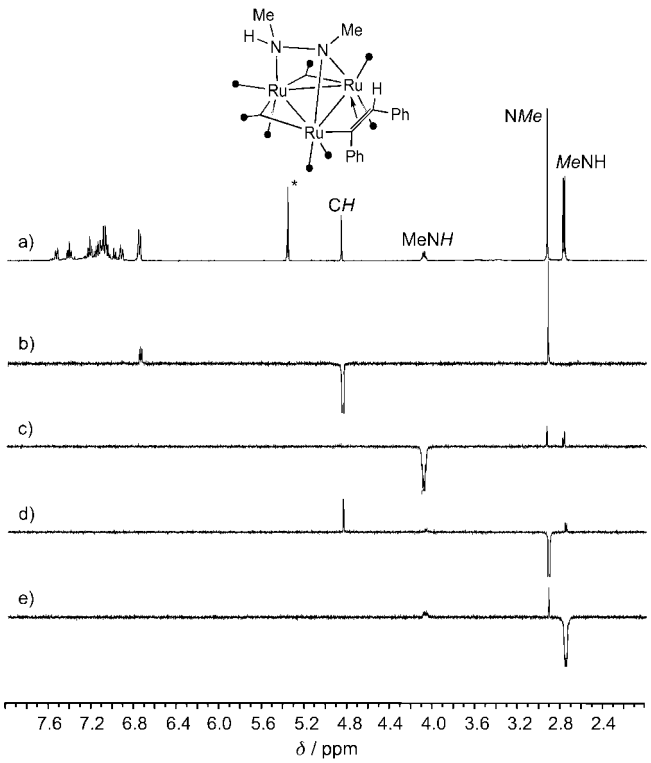

Figure 6. ^{1}H NMR spectrum (CD_2Cl_2, 20 °C, 400 MHz) of **18** (a) and difference ^{1}H NOE NMR spectra after presaturation at the frequencies of the C*H* (b), MeN*H* (c), N*Me* (d), and *Me*NH (e) resonances. The peak marked with an asterisk is due to residual CH_2Cl_2 solvent.

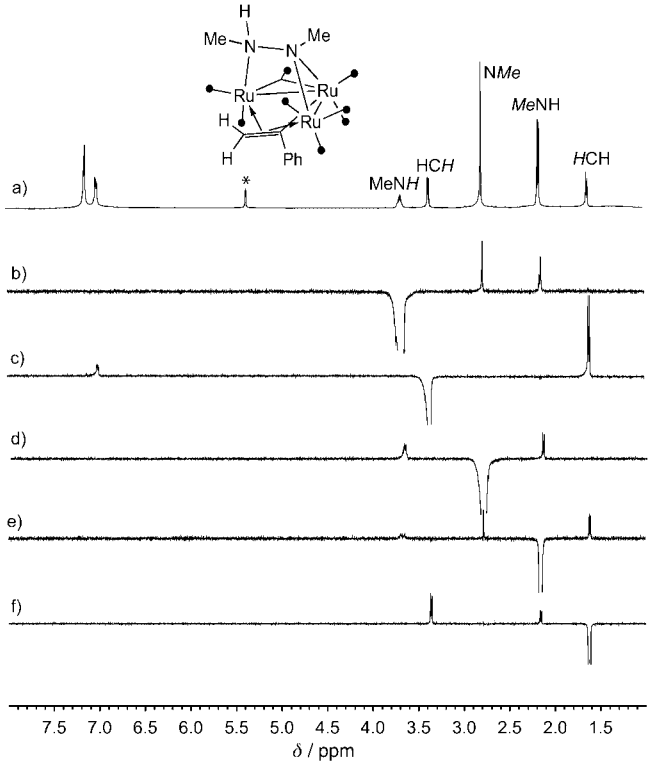

Figure 7. ^{1}H NMR spectrum (CD_2Cl_2, 20 °C, 400 MHz) of **21** (a) and difference ^{1}H NOE NMR spectra after presaturation at the frequencies of the MeN*H* (b), HC*H* (c), N*Me* (d), *Me*NH (e), and *H*CH (f) resonances. The peak marked with an asterisk is due to residual CH_2Cl_2 solvent.

Calculated structures are assigned Roman numbers, irrespectively of whether they correspond to real (designated by Arabic numbers) or hypothetical compounds. Computer-generated images of all these structures and lists of atomic coordinates are given as Supporting Information.

For the cases in which both experimental (X-ray diffraction) and theoretical (DFT calculations) structural data were obtained, the bond lengths and angles given by both methods are practically identical. This fact validates the calculations.

Scheme 5 shows the calculated energies of structures belonging to two families of isomeric compounds, formally derived from reactions of diphenylacetylene and acetylene with **1**. For both alkynes, structure **I**, which corresponds to species in which the amido and alkenyl fragments span the same Ru–Ru edge, is much more stable (by >10 kcal mol^{-1}) than structure **II**, which corresponds to species in which the amido and alkenyl fragments span different Ru–Ru edges. This explains why all the isolated products derived from **1** that contain an edge-bridging alkenyl ligand have the ligand arrangement of structure **I**. For face-capping derivatives of both alkynes, asymmetric structure **III** is much more stable than symmetric **IV**. This supports the fact that no symmetric compounds containing face-capping alkenyl ligands have been experimentally obtained. Whereas the acetylene-derived structures **Ib** and **IIIb** have similar energies (they only differ by 0.68 kcal mol^{-1}), the diphenyl derivative **Ia** is 3.84 kcal mol^{-1} more stable than **IIIa**. Therefore, different alkynes may result in minimum-energy products with different isomeric structures. In fact, compounds **3** and **7**, which are the only products of the reactions of **1** with diphenylacetylene and acetylene, respectively, have different structures.

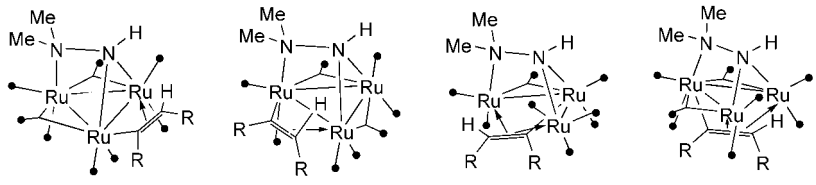

Scheme 5. Relative energies [kcal mol^{-1}] of DFT-calculated minimum-energy structures of isomeric products formally derived from reactions of diphenylacetylene and acetylene with **1**. The energy of the most stable structure of each family of isomers is assigned as 0.00 kcal mol^{-1}.

When terminal alkynes are used, their alkenyl products can have a *gem* or a *trans* arrangement of their two H atoms. Scheme 6 shows the relative energies of DFT-optimized structures of four isomeric products derived from methyl propiolate and **1** (structures analogous to **II** and **IV** were not calculated because they were expected to be less stable; see above). These energies clearly indicate

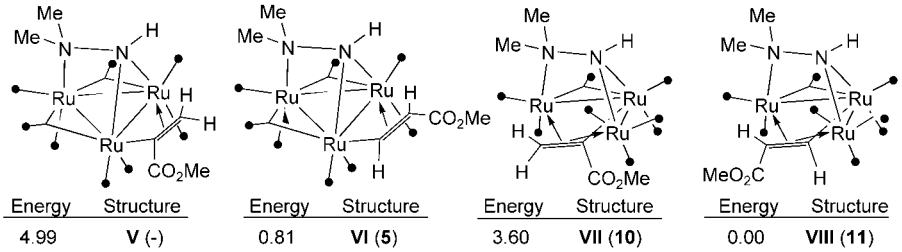

Scheme 6. Relative energies [kcal mol^{-1}] of DFT-optimized structures of isomeric products formally derived from methyl propiolate and **1**. The energy of the most stable structure is assigned as 0.00 kcal mol^{-1}.

that *trans*-alkenyl products are thermodynamically more stable than *gem*-alkenyl derivatives, both for edge-bridging and face-capping situations.

The asymmetry of the bridging hydrazido ligand of compound **2** increases the number of possible isomeric alkenyl derivatives. Scheme 7 shows the calculated minimum-energy structures of edge-bridging and face-capping isomers formally derived from reactions of phenylacetylene and acetylene with **2**. For both alkynes, structures **IX**, **XI,** and **XIV** are the most stable and correspond to the three isomeric products experimentally obtained from the reactions of **2** with phenylacetylene (**16**, **19,** and **21**) and acetylene (**17**, **20,** and **22**). The energies of the phenylacetylene-derived structures **IXa**, **XIa,** and **XIVa** are very close to each other (the least stable, **IXa**, is only 0.51 kcal mol^{-1} above the most stable, **XIa**). However, for the acetylene-derived compounds, structure **XIb** is 2.89 kcal mol^{-1} less stable than **XIVb**. Therefore, changes in the R substituents of the alkenyl fragments may induce important changes in the relative stability of their isomeric products.

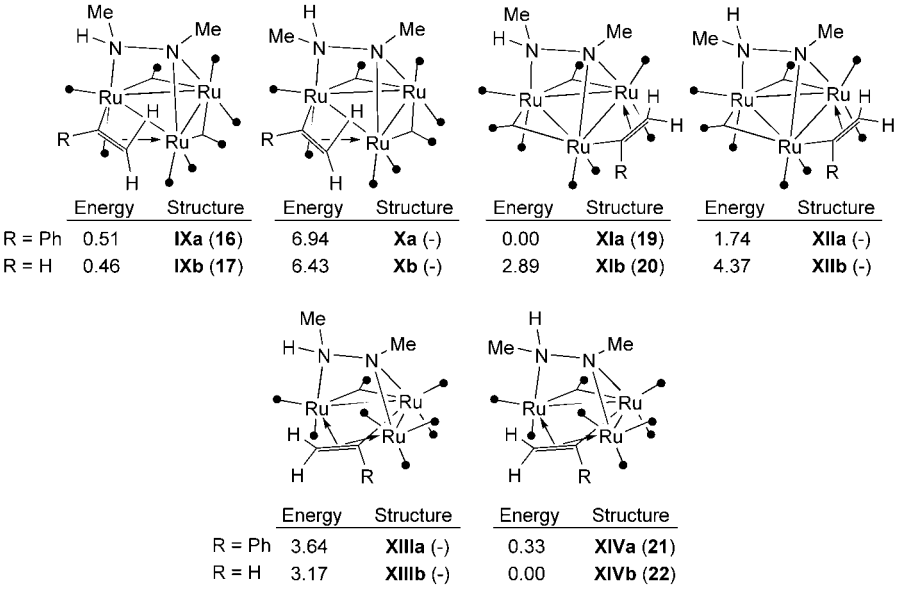

Scheme 7. Relative energies [kcal mol^{-1}] of DFT-optimized structures of isomeric products formally derived from reactions of phenylacetylene and acetylene with **2**. The energy of the most stable structure of each family of isomers is assigned as 0.00 kcal mol^{-1}.

From these calculations, it can be concluded that, for edge-bridged alkenyl derivatives, the least stable structures are those in which a methyl group of the MeNMe or MeNH fragment is adjacent to the alkenyl-bridged Ru–Ru edge (**II** and **X**). In fact, such compounds have not been experimentally observed. In this context, it is curious that, for the face-capped alkenyl derivatives of **2**, the most stable structures are those in which the methyl group of the MeNH fragment is adjacent to the open Ru–Ru edge (**XIV**). Thus, on going from structures **XIV** to **XIII**, which implies an exchange of the H and Me groups of the MeNH fragment, the energy increases by 3.31 (R = Ph, **XIIIa**) and 3.17 kcal mol^{-1} (R = H, **XIIIb**).

As mentioned above, within the family of face-capped alkenyl products, the IR spectra of complexes **13**, **14,** and **23** are appreciably different (Table 5, Figure 5) from those of the majority of the members of this family (Table 4, Figure 5), the major difference being that the former contain two absorptions due to bridging carbonyls, whereas the latter contain only one. X-ray diffraction (**10**–**12**) and DFT calculations (**7**, **10**, **11**, **21,** and **22**) confirmed the presence of only one bridging CO ligand in the compounds of the major group. As no X-ray diffraction data could be obtained for **13**, **14,** and **23**, their structure was elucidated by DFT calculations. As a representative example, the minimum-energy structure of $[Ru_3(\mu_3\text{-}\eta^2\text{-}HNNMe_2)(\mu_3\text{-}\eta^2\text{-}HCCHPh)(\mu\text{-}CO)_2(CO)_6]$ (**13**, structure **XV**) is shown in Figure 8. A selection of interatomic distances is given in Table 2. This structure is the output of a calculation for which the input was the optimized structure of **11** (**VII**), which contains only one bridging CO ligand, appropriately modified by substituting a phenyl group for the original CO_2Me group. Overall, the calculated structure of **13** is very similar to that of **11**, the major differences between them being that the Ru1–Ru3 and C4–Ru1 distances are 0.14 and 0.22 Å, respectively, longer in **13** than in **11**, and that the C11O11 carbonyl ligand asymmetrically spans the Ru1–Ru2 edge of **13** (C11–Ru1 2.018, C11–Ru2 2.249 Å), whereas it is terminal in **11**. Therefore, within the family of face-capped alkenyl complexes, noticeable structural changes in the attachment of the CO ligands to the metal atoms can be provoked by subtle changes in the nature of the alkenyl ligands, such as the *gem* to *trans* arrangement of the alkenyl

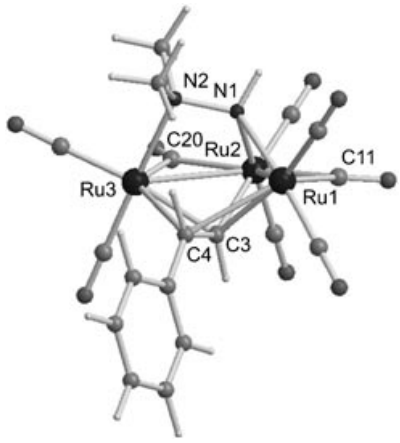

Figure 8. DFT-optimized molecular structure of **13** (structure **XV**).

hydrogen atoms, for example, **9** (*gem*, one bridging CO ligand) and **13** (*trans*, two bridging CO ligands), or different R substituents on the alkenyl fragment while maintaining the positions of the hydrogen atoms, for example, **11** (*trans*, R = CO_2Me, one bridging CO ligand) and **13** (*trans*, R = Ph, two bridging CO ligands).

Kinetic studies: To shed light on the mechanistic aspects of these reactions, the kinetics of the reaction of **1** with diphenylacetylene were studied as a representative example.

Kinetic data were obtained under pseudo-first-order conditions ([Ph_2C_2] ≫ [**1**]), by measuring the disappearance of the IR absorption at 2081 cm^{-1} of **1** as a function of time (details are given in the Experimental Section). The results indicate that the reaction is first-order in the concentration of trinuclear complex and first-order in alkyne concentration, with a rate law of the type $v = k_2[Ph_2C_2][\mathbf{1}]$. Second-order rate constants k_2 and activation parameters ($\Delta H^{\neq}$ and $\Delta S^{\neq}$) are given in Table 7.

Table 7. Second-order rate constants and activation parameters for the reaction of **1** with Ph_2C_2.

T [K]	$10^4\,k_2$ [$s^{-1}\,mol^{-1}\,L$]	$\Delta H^{\neq}$ [kcal mol^{-1}]	$\Delta S^{\neq}$ [cal $K^{-1}\,mol^{-1}$]
318	6.4	14 ± 2	−32 ± 1
328	9.6		
338	19.2		
348	49.6		

Second-order kinetics, small $\Delta H^{\neq}$, and negative $\Delta S^{\neq}$ are consistent with an associative mechanism.[14] Although a reaction pathway in which the addition of the alkyne is preceded by a pre-equilibrium that involves cleavage of a bond (Ru–Ru or Ru–N) to create a vacant site in the cluster would also follow second-order kinetics, the experimental $\Delta H^{\neq}$ is too low for such a process, for which $\Delta H^{\neq}$ would be sum of the bond energy of the broken bond and the activation barrier for attack of the alkyne on the coordinatively unsaturated metal atom.[15]

Only one previous mechanistic study on reactions of trinuclear carbonyl clusters containing face-capping N-donor ligands has been reported.[15] It deals with reactions of phosphane ligands with anionic complexes of the type [PPN][$Ru_3(\mu_3\text{-}\eta^2\text{-}Xpy)(\mu\text{-}CO)_3(CO)_6$] (X = S, NMe, NPh). These reactions also follow second-order kinetics, and it was proposed that they take place by an associative mechanism in which attack of the phosphane on the metal atom is accompanied by cleavage of an Ru–X bond. A subsequent CO loss would reform the Ru–X bond and yield the monosubstituted product.[15]

Although a mechanism of this type could also be proposed for the first step of the reactions described here, an alternative proposal in which the attack of the entering ligand is concomitant with a lengthening of several bonds of the cluster, and not with cleavage of a localized Ru–X bond, would also be possible.[16] Such a proposal is substantiated by a few reports that describe closed, trinuclear, ligand-bridged, 50-electron, carbonyl clusters of ruthenium[17] and osmium[18] in which the three M–M distances are longer than expected for normal single bonds but shorter than open M···M edges.

Unfortunately, the fact that the rate-limiting step is the first step of the reaction pathway (the remaining steps are faster and occur later) prevented the isolation and/or characterization of reaction intermediates that could shed more light on how the final alkenyl products are formed.

Discrepancies with the results of Hansert and Vahrenkamp: A comparison of our results and those reported by Hansert and Vahrenkamp[4] (summarized in Scheme 2 and in the Introduction) reveals many discrepancies.

For certain reagents, the number of products obtained by the two groups is different. This may be due to the use of different reaction and/or separation conditions. But it is curious that in no case did they obtain any *trans* alkenyl product derived from phenylacetylene, as we have done.

The most important discrepancies correspond to structural assignments. Hansert and Vahrenkamp had the problem of having three different products from their reactions, of which one was clearly face-capped (IR) but the other two had very similar IR spectra (as stated above, the IR spectra of all the edge-bridged alkenyl products are very similar in the carbonyl stretching region). They also had the X-ray structure of **16** (structure **A** in Scheme 2). On the basis of these data, they divided their edge-bridged alkenyl products into two groups, one for the products of structure **A**, and the other for products of unknown structure (compounds **C** in Scheme 2, which Hansert and Vahrenkamp said had nine CO ligands). As a consequence of the lack of a clear differentiating criterion to make such a classification, they assigned structure **A** to compounds that in fact do not have that structure, for example, **3**, **18**, and **19**, in which the alkenyl ligand and the amido fragment span the same edge of the metal triangle, and included complex **15**, which has structure **A**, in group **C**.

We encountered an additional problem when we tried to elucidate the true structures of the compounds described by Hansert and Vahrenkamp. When comparing IR and NMR data, we found that the data for some of their compounds did not match those of any of our compounds. Furthermore,

they reported the X-ray structure of **16** but, curiously, the reported spectroscopic data of this compound matched our data for **19**. In addition, our data for **16** matched their data for a compound they tentatively formulated as $[Ru_3(\mu_2\text{-}\eta^2\text{-}MeNNHMe)(\mu\text{-}\eta^2\text{-}PhCCH_2)(CO)_9]$ and assigned to group **C** (Scheme 2). To further clarify the situation, we determined the X-ray structure of the compound with those spectroscopic data, and the structure of **16** resulted, confirming that our spectroscopic data were correct.

Conclusion

Very few reactions of alkynes with face-capped hydrido triruthenium clusters had been previously reported. Diphenylacetylene was the most widely used alkyne by us[1] and Lavigne et al.[2] in reactions with clusters derived from 2-aminopyridines. Curiously, these reactions are regioselective in the sense that they give only one product, an edge-bridged alkenyl derivative. Other internal and terminal alkynes were used by Süss-Fink et al. in reactions with $[Ru_3(\mu\text{-}H)\{\mu_3\text{-}NS(O)MePh\}(CO)_9]$. They observed mixtures of various isomeric edge-bridged and face-capped alkenyl products, partly as a consequence of the asymmetry of the bridging sulphoximido ligand.[3a] In none of these previous studies were the results rationalized in terms of the kinetic and/or thermodynamic stability of the possible isomeric products.

The results reported here represent a rather broad picture of the reactivity of alkynes with hydrazido-bridged hydrido-triruthenium carbonyl clusters and complement previous data on the reactivity of alkynes with triruthenium carbonyl clusters containing other face-capping ligands. We have shown that the selectivity of the reactions is influenced by the nature of both the face-capping ligand and the alkyne reagent. Density functional calculations helped us to deduce that the products of the reactions that give a single product (those of **1** with diphenylacetylene and acetylene) are the most stable ones among the possible isomeric products (Scheme 5), and that the products of the reactions that give mixtures of isomers have similar thermodynamic stabilities and include the most stable product of the possible isomeric products (Schemes 6 and 7). Therefore, the kinetic aspects of the migratory insertion processes (formation of the alkenyl ligands) have little influence on the selectivity of the reactions. This implies that, at short reaction times and/or at low temperatures, when different alkenyl products are formed, none of them is an intermediate in the formation of any of the others; in other words, they are all formed, through pathways that have similar activation energies, from a common unstable hydrido alkyne intermediate that arises from coordination of the alkyne to **1** or **2**. A kinetic study demonstrated that the formation of this intermediate follows an associative pathway and that this process is the rate-limiting step of the overall reaction. We also showed that *gem*-alkenyl products can be converted into *trans*-alkenyl products, but this transformation has a higher activation energy than the formation of the *trans* or *gem* products directly from the hydrido alkyne intermediate.

Despite the great deal of information contained in this article on the reactivity of hydrazido-capped hydrido triruthenium carbonyl clusters with alkynes, some questions are still open. Why, among the possible isomeric products of a reaction, is one more stable than the others? Why are the complexes that contain face-capping alkenyl ligands open clusters (two Ru–Ru bonds), contrary to the predictions of the EAN rules for trinuclear 48-electron species? The answers to these questions will require in-depth theoretical calculations that we leave for forthcoming research.

Experimental Section

General: Solvents were dried over $Na[Ph_2CO]$ (THF, diethyl ether, hydrocarbons), or CaH_2 (dichloromethane, 1,2-dichloroethane) and distilled under nitrogen prior to use. The reactions were carried out under nitrogen by using Schlenk/vacuum line techniques and were routinely monitored by solution IR spectroscopy and by spot TLC on silica gel. Compounds **1** and **2** were prepared as described elsewhere.[4,7] IR: Perkin-Elmer FT Paragon 1000X. NMR: Bruker AV-400 and DPX-300, room temperature, TMS as internal standard ($\delta = 0$). Microanalyses: Perkin-Elmer 2400. MS: VG Autospec double-focusing mass spectrometer operating in the FAB+ mode; ions were produced with a standard Cs^+ gun at ca. 30 kV; 3-nitrobenzyl alcohol (NBA) was used as matrix. All isolated products gave satisfactory C, H, N, microanalyses (Supporting Information). All their FAB+ mass spectra showed the corresponding molecular ion (Supporting Information).

The following description of the reactions of compounds **1** and **2** with alkynes is arranged in alphabetical order of the alkyne name.

Reaction of 1 with acetylene: synthesis of $[Ru_3(\mu_3\text{-}\eta^2\text{-}HNNMe_2)(\mu_3\text{-}\eta^2\text{-}HCCH_2)(\mu\text{-}CO)(CO)_7]$ (7): Acetylene was gently bubbled through a solution of **1** (50 mg, 0.081 mmol) in THF (30 mL) at reflux for 20 min. The color changed from yellow to orange. The solvent was removed under reduced pressure and the residue was crystallized from dichloromethane/hexane to give **7** as an brownish orange solid (44 mg, 89%).

Reaction of 1 with dimethyl acetylenedicarboxylate: synthesis of $[Ru_3(\mu_3\text{-}\eta^2\text{-}HNNMe_2)(\mu_3\text{-}\eta^2\text{-}MeO_2CCCHCO_2Me)(\mu\text{-}CO)(CO)_7]$ (8): A solution of **1** (50 mg, 0.081 mmol) and dimethyl acetylenedicarboxylate (10 μL, 0.089 mmol) in THF (20 mL) was stirred under reflux for 20 min. The color changed from yellow to dark orange. The solvent was removed under reduced pressure and the residue was separated by TLC (silica gel) with hexane/THF (4/1) as eluant. Extraction of the major band (third, orange) allowed the isolation of **8** as an orange solid (28 mg, 47%).

Reaction of 1 with diphenylacetylene: synthesis of $[Ru_3(\mu_3\text{-}\eta^2\text{-}HNNMe_2)(\mu\text{-}\eta^2\text{-}PhCCHPh)(\mu\text{-}CO)_2(CO)_6]$ (3): A solution of **1** (50 mg, 0.081 mmol) and diphenylacetylene (17 mg, 0.089 mmol) in THF (30 mL) was stirred under reflux for 85 min. The color changed from yellow to red. The solvent was removed under reduced pressure and the residue was crystallized from dichloromethane/hexane to give **3** as a red solid (49 mg, 79%).

Reaction of 1 with 2-ethynylpyridine: synthesis of $[Ru_3(\mu_3\text{-}\eta^2\text{-}HNNMe_2)(\mu\text{-}\eta^2\text{-}pyCCH_2)(\mu\text{-}CO)_2(CO)_6]$ (6) and $[Ru_3(\mu_3\text{-}\eta^2\text{-}HNNMe_2)(\mu_3\text{-}\eta^3\text{-}HCCHpy)(\mu\text{-}CO)(CO)_7]$ (12): A solution of **1** (100 mg, 0.162 mmol) and 2-ethynylpyridine (18 μL, 0.178 mmol) in THF (40 mL) was stirred under reflux for 12 min. The color changed from yellow to orange. The solvent was removed under reduced pressure, the residue was dissolved in dichloromethane (2 mL), and the resulting solution was supported on a silica gel chromatographic column (3×20 cm) packed in hexane. Hexane/dichloromethane (1/1) eluted four bands. The first three were very weak and were not collected. The fourth band contained **12**, which was isolated as a red solid after solvent removal (13 mg, 12%). Further elution of the column with dichloromethane afforded an orange band, which contained a mixture of compounds. This mixture was separated by TLC (silica gel). Repeated elution with hexane/dichloromethane

(1/1) allowed the separation of the major band, which, after workup, afforded **6** as an orange solid (19 mg, 17%).

Reaction of 1 with 2-methylbut-3-yn-2-ol: synthesis of [$Ru_3(\mu_3\text{-}\eta^2\text{-}HNNMe_2)(\mu\text{-}\eta^2\text{-}HOMe_2CCCH_2)(\mu\text{-}CO)_2(CO)_6$] (4) and [$Ru_3(\mu_3\text{-}\eta^2\text{-}HNNMe_2)(\mu_3\text{-}\eta^2\text{-}HCCHCMe_2OH)(\mu\text{-}CO)_2(CO)_6$] (14): A solution of **1** (50 mg, 0.081 mmol) and 2-methylbut-3-yn-2-ol (9 μL, 0.089 mmol) in THF (20 mL) was stirred under reflux for 15 min. The color changed from yellow to orange. The solvent was removed under reduced pressure and the residue was separated by TLC (silica gel). Hexane/dichloromethane (1/1) eluted two bands. Compound **4** was extracted from the first band and was isolated as an orange solid (8 mg, 12%). Compound **14** was extracted from the second band and was isolated as dark yellow solid (21 mg, 39%). A dark residue remained uneluted in the base line.

Reaction of 1 with methyl propiolate: synthesis of [$Ru_3(\mu_3\text{-}\eta^2\text{-}HNNMe_2)(\mu\text{-}\eta^2\text{-}HCCHCO_2Me)(\mu\text{-}CO)_2(CO)_6$] (5), [$Ru_3(\mu_3\text{-}\eta^2\text{-}HNNMe_2)(\mu_3\text{-}\eta^2\text{-}MeO_2CCCH_2)(\mu\text{-}CO)(CO)_7$] (10), and [$Ru_3(\mu_3\text{-}\eta^2\text{-}HNNMe_2)(\mu_3\text{-}\eta^2\text{-}HCCHCO_2Me)(\mu\text{-}CO)(CO)_7$] (11): A solution of **1** (100 mg, 0.162 mmol) and methyl propiolate (16 μL, 0.179 mmol) in THF (30 mL) was stirred under reflux for 30 min. The color changed from yellow to orange. The solvent was removed under reduced pressure, the residue was dissolved in dichloromethane (2 mL), and the resulting solution was supported on a silica gel chromatographic column (3×20 cm) packed in hexane. Hexane/dichloromethane (3/2) eluted **10**, which was isolated as an orange solid after solvent removal (47 mg, 43%). Hexane/dichloromethane (2/3) eluted **11**, which was isolated as an orange solid after solvent removal (18 mg, 16%). Hexane/dichloromethane (1/4) eluted **5**, which was isolated as an orange solid after solvent removal (7 mg, 6%).

Reaction of 1 with phenylacetylene: synthesis of [$Ru_3(\mu_3\text{-}\eta^2\text{-}HNNMe_2)(\mu_3\text{-}\eta^2\text{-}PhCCH_2)(\mu\text{-}CO)(CO)_7$] (9) and [$Ru_3(\mu_3\text{-}\eta^2\text{-}HNNMe_2)(\mu_3\text{-}\eta^2\text{-}HCCHPh)(\mu\text{-}CO)_2(CO)_6$] (13): A solution of **1** (50 mg, 0.081 mmol) and phenylacetylene (10 μL, 0.089 mmol) in THF (20 mL) was stirred under reflux for 20 min. The color changed from yellow to red. The solvent was removed under reduced pressure. A ^{1}H NMR spectrum of the residue indicated the presence of **9** and **13** in a 3/1 ratio. The solid residue was recrystallized twice from dichloromethane/hexane to give **9** as an orange solid (32 mg, 57%). Compound **13** was best prepared by heating under reflux a solution of a 3/1 mixture of **9** and **13** (50 mg, 0.072 mmol) in toluene (10 mL) for 10 min. The solvent was removed under reduced pressure and the solid residue was recrystallized twice from dichloromethane/hexane to give the product as an orange solid (36 mg, 65%).

Reaction of 2 with acetylene: synthesis of [$Ru_3(\mu_3\text{-}\eta^2\text{-}MeNNHMe)(\mu\text{-}\eta^2\text{-}HCCH_2)(\mu\text{-}CO)_2(CO)_6$] (isomers 17 and 20) and [$Ru_3(\mu_3\text{-}\eta^2\text{-}MeNNHMe)(\mu_3\text{-}\eta^2\text{-}HCCH_2)(\mu\text{-}CO)(CO)_7$] (22): Acetylene was gently bubbled through a solution of **2** (50 mg, 0.081 mmol) in THF (30 mL) under reflux for 20 min. The color changed from yellow to orange. The solvent was removed under reduced pressure and the residue was separated by TLC (silica gel) with hexane/dichloromethane (2/1) as eluant. The bands were extracted to give, in order of elution, **17** (orange solid, 15 mg, 30%), **20** (orange solid, 5 mg, 10%), and **22** (yellow solid, 17 mg, 34%).

Reaction of 2 with diphenylacetylene: synthesis of [$Ru_3(\mu_3\text{-}\eta^2\text{-}MeNNHMe)(\mu\text{-}\eta^2\text{-}PhCCHPh)(\mu\text{-}CO)_2(CO)_6$] (isomers 15 and 18) and [$Ru_3(\mu_3\text{-}\eta^2\text{-}MeNNHMe)(\mu_3\text{-}\eta^2\text{-}PhCCHPh)(\mu\text{-}CO)_2(CO)_6$] (23): A solution of **2** (50 mg, 0.081 mmol) and diphenylacetylene (17 mg, 0.089 mmol) in THF (30 mL) was stirred under reflux for 35 min. The color changed from yellow to dark orange. The solvent was removed under reduced pressure and the residue was separated by TLC (silica gel) with hexane/dichloromethane (5/1) as eluant. Three bands were eluted and extracted to give, in order of elution, **23** (yellow solid, 6 mg, 10%), **18** (red solid, 12 mg, 19%), and **15** (orange solid, 14 mg, 23%).

Reaction of 2 with phenylacetylene: synthesis of [$Ru_3(\mu_3\text{-}\eta^2\text{-}MeNNHMe)(\mu\text{-}\eta^2\text{-}PhCCH_2)(\mu\text{-}CO)_2(CO)_6$] (isomers 16 and 19) and [$Ru_3(\mu_3\text{-}\eta^2\text{-}MeNNHMe)(\mu_3\text{-}\eta^2\text{-}PhCCH_2)(\mu\text{-}CO)(CO)_7$] (21): A solution of **2** (50 mg,

Table 8. Crystal, measurement, and refinement data for the compounds studied by X-ray diffraction.

	3	**5**	**10**	**11**	**12**	**15**
formula	$C_{24}H_{18}N_2O_8Ru_3$	$C_{14}H_{12}N_2O_{10}Ru_3$	$C_{14}H_{12}N_2O_{10}Ru_3$	$C_{14}H_{12}N_2O_{10}Ru_3$	$C_{17}H_{13}N_3O_8Ru_3$	$C_{24}H_{18}N_2O_8Ru_3$
formula weight	765.61	671.47	671.47	671.47	690.51	765.61
crystal system	triclinic	triclinic	triclinic	monoclinic	orthorhombic	monoclinic
space group	$P\bar{1}$	$P\bar{1}$	$P\bar{1}$	$P2_1/c$	$P2_12_12_1$	$P2_1/c$
a [Å]	7.6934(3)	7.6473(4)	9.0089(5)	8.7734(3)	8.9655(4)	10.5421(3)
b [Å]	11.6631(4)	10.4687(5)	9.7582(6)	14.2762(4)	12.1096(4)	14.9160(5)
c [Å]	15.7483(7)	12.8350(7)	13.1095(8)	15.9178(6)	18.8958(6)	16.8300(6)
α [°]	77.942(2)	88.160(3)	104.617(4)	90	90	90
β [°]	88.696(3)	73.622(4)	93.472(3)	95.045(2)	90	96.412(2)
γ [°]	71.927(3)	82.343(3)	116.430(3)	90	90	90
V [Å^3]	1312.38(9)	977.03(9)	978.53(9)	1986.0(1)	2051.5(1)	2629.8(2)
Z	2	2	2	4	4	4
F(000)	744	644	644	1288	1328	1488
ρ_{calcd} [g cm^{-3}]	1.937	2.282	2.279	2.246	2.236	1.934
radiation (λ [Å])	$Cu_{K\alpha}$ (1.54180)	$Cu_{K\alpha}$ (1.54180)	$Cu_{K\alpha}$ (1.54180)	$Cu_{K\alpha}$ (1.54180)	$Cu_{K\alpha}$ (1.54180)	$Cu_{K\alpha}$ (1.54180)
μ [mm^{-1}]	14.241	19.068	19.039	18.762	18.131	14.213
crystal size [mm]	0.13×0.10×0.05	0.20×0.10×0.08	0.15×0.15×0.03	0.15×0.10×0.08	0.15×0.10×0.08	0.33×0.08×0.05
T [K]	120(2)	120(2)	200(2)	120(2)	120(2)	150(2)
θ limits [°]	2.87–68.69	3.59–68.34	3.56–68.75	4.17–68.50	4.34–68.28	4.22–68.24
min./max. h, k, l	0/9, −12/14, −18/18	0/9, −12/12, −14/15	−10/10, −11/11, −15/15	−10/10, −15/17, −19/19	−9/10, −14/14, −22/22	−12/12, −17/17, −20/20
collected reflns	17416	7017	6015	16839	18796	9158
unique reflns	4803	3530	3582	3654	3617	4786
reflns with $I>2\sigma(I)$	4474	3189	3101	3192	3392	3827
absorption correction	XABS2	XABS2	XABS2	XABS2	SORTAV	XABS2
max./min. transmission	0.491/0.228	0.236/0.155	0.625/0.135	0.223/0.105	0.655/0.499	0.490/0.294
parameters/restraints	340/1	265/0	271/3	273/0	274/0	334/1
GOF on F^2	1.177	1.171	1.029	1.089	1.003	1.118
R_1 (on F, $I>2\sigma(I)$)	0.0491	0.0567	0.0594	0.0297	0.0473	0.0666
wR_2 (on F^2, all data)	0.1869	0.240	0.1636	0.0852	0.1643	0.2670
max./min. $\Delta\rho$ [e Å^{-3}]	1.602/−1.477	1.867/−2.180	1.911/−2.144	1.131/−0.826	1.243/−1.704	1.346/2.283

0.081 mmol) and phenylacetylene (10 μL, 0.089 mmol) in THF (30 mL) was stirred under reflux for 15 min. The color changed from yellow to bright orange. The solvent was removed under reduced pressure and the residue was separated by TLC (silica gel) with hexane/dichloromethane (5/1) as eluant. Three bands were eluted and extracted to give, in order of elution, **21** (yellow solid, 15 mg, 27%), **19** (red solid, 10 mg, 18%), and **16** (orange solid, 16 mg, 29%).

X-ray structures of 3, 5, 10, 11, 12, and 15: Diffraction data were collected on a Nonius Kappa-CCD diffractometer using graphite-monochromated $Cu_{K\alpha}$ radiation. Data were reduced to F_o^2 values. Absorption corrections were applied using XABS2[19] for **3**, **5, 10**, **11**, and **15**, and SORTAV[20] for **12**. Structures were solved by Patterson interpretation using the program DIRDIF-96.[21] Isotropic and full-matrix anisotropic least-squares refinements were carried out using SHELXL-97.[22] The C1, C20, and C42 carbon atoms of **12** and the H atoms of all structures were refined with isotropic thermal parameters. All remaining non-H atoms were refined anisotropically. The molecular plots were made with the EUCLID program package.[23] The WINGX program system[24] was used throughout the structure determinations. Crystal, measurement, and refinement data for the compounds studied by X-ray diffraction are listed in Table 8.

CCDC-238358 (**3**), CCDC-238359 (**5**), CCDC-238360 (**10**), CCDC-238361 (**11**), CCDC-238362 (**12**), and CCDC-238363 (**15**) contain the supplementary crystallographic data for this paper. These data can be obtained free of charge via www.ccdc.cam.ac.uk/conts/retrieving.html (or from the Cambridge Crystallographic Data Centre, 12 Union Road, Cambridge CB21EZ, UK; fax: (+44) 1223-336-033; or deposit@ccdc.cam.uk).

Kinetic measurements: All kinetic experiments were run under pseudo-first-order conditions at a $[Ph_2C_2]/[\mathbf{1}]$ ratio of at least 15. Data were obtained by measuring the disappearance of the IR absorption of **1** at 2081 cm^{-1}. The spectra were recorded in absorbance mode on a Perkin-Elmer FT Paragon 1000 spectrophotometer using a Specac P/N 21525 variable-temperature cell with 0.5 mm-spaced NaCl windows. In each experiment, **1** (10 mg, 0.016 mmol) and the appropriate amount of diphenylacetylene were dissolved in cold (0°C), dry, and deoxygenated toluene (total volume 10 mL). A portion of this solution was transferred with a syringe to the IR cell, which was previously preheated to the appropriate temperature. After an equilibration time of 2 min, the absorbance of the IR absorption at 2081 cm^{-1} was recorded every 2 min for 20 min. Plots of $\ln A_t$ (A_t is the absorbance at time t) vs time were linear for all reactions ($r^2 > 0.99$). The slopes of these lines yielded the observed rate constants k_{obs}. Plots of k_{obs} vs $[Ph_2C_2]$ at each temperature were also linear ($r^2 > 0.95$). Second-order rate constants k_2 were calculated from the slopes of these lines ($k_{obs} = k_2[Ph_2C_2]$ when $[Ph_2C_2] \gg [\mathbf{1}]$). Activation parameters were derived from the Eyring equation.

Theoretical calculations: All the minimum-energy structures reported herein were optimized by hybrid DFT within the Gaussian 98 program suite[25] by using Becke's three-parameter hybrid exchange-correlation functional[26] containing the nonlocal gradient correction of Lee, Yang, and Parr (B3LYP).[27] The Hay–Wadt Los Alamos National Laboratory two-shell double-ζ (LANL2DZ) basis set, with relativistic effective core potentials, was used for the Ru atoms.[28] The basis set used for the remaining atoms was 6-31G with addition of (d,p) polarization for all atoms. All optimized structures were confirmed as minima by calculation of analytical frequencies. For each calculation, the input model molecule was based on one of the X-ray structures reported in this article, conveniently modified by changing the appropriate R groups.

Acknowledgement

This work has been supported by the Spanish DGESIC (grant PB98-1555), CICYT (grants BQU2003-5093 and BQU2002-2623), and Principado de Asturias (grants PR-01-GE-7 and PR-01-GE-4).

[1] a) J. A. Cabeza, S. García-Granda, A. Llamazares, V. Riera, J. F. Van der Maelen, *Organometallics* **1993**, *12*, 157; b) J. A. Cabeza, S. García-Granda, A. Llamazares, V. Riera, J. F. Van der Maelen, *Organometallics* **1993**, *12*, 2973; c) P. Briard, J. A. Cabeza, A. Llamazares, L. Ouahab, V. Riera, *Organometallics* **1993**, *12*, 1006; d) S. Alvarez, P. Briard, J. A. Cabeza, I. del Río, J. M. Fernández-Colinas, F. Mulla, L. Ouahab, V. Riera, *Organometallics* **1994**, *13*, 4360; e) J. A. Cabeza, A. Llamazares, V. Riera, P. Briard, L. Ouahab, *J. Organomet. Chem.* **1994**, *480*, 205; f) J. A. Cabeza, J. M. Fernández-Colinas, A. Llamazares, V. Riera, S. García-Granda, J. F. Van der Maelen, *Organometallics* **1994**, *13*, 4352.

[2] a) N. Lugan, F. Laurent, G. Lavigne, T. P. Newcomb, E. W. Liimatta, J. J. Bonnet, *Organometallics* **1992**, *11*, 1351; b) P. Nombel, N. Lugan, F. Mulla, G. Lavigne, *Organometallics* **1994**, *13*, 4673; P. Nombel, N. Lugan, B. Donnadieu, G. Lavigne, *Organometallics* **1999**, *18*, 187.

[3] a) V. Ferrand, K. Merzweiler, G. Rheinwald, H. Stoeckli-Evans, G. Süss-Fink, *J. Organomet. Chem.* **1997**, *549*, 263; b) V. Ferrand, A. Neels, H. Stoeckli-Evans, G. Süss-Fink, *Inorg. Chem. Commun.* **1999**, *2*, 561; c) V. Ferrand, C. Gambs, N. Derrien, C. Bolm, H. Stoeckli-Evans, G. Süss-Fink, *J. Organomet. Chem.* **1997**, *549*, 275.

[4] B. Hansert, H. Vahrenkamp, *Chem. Ber.* **1993**, *126*, 2017.

[5] N. Lugan, F. Laurent, G. Lavigne, T. P. Newcomb, E. W. Liimatta, J. J. Bonnet, *J. Am. Chem. Soc.* **1990**, *112*, 8607.

[6] For reviews on alkyne hydrogenation mediated by triruthenium carbonyl cluster complexes, see a) J. A. Cabeza in *Metal Clusters in Chemistry* (Eds.: P. Braunstein, L. A. Oro, P. R. Raithby), Wiley-VCH, Weinheim, **1999**, p. 715; b) J. A. Cabeza, J. M. Fernández-Colinas, A. Llamazares, *Synlett* **1995**, 579.

[7] T. Jenke, H. Stoeckli-Evans, G. Süss-Fink, *J. Organomet. Chem.* **1990**, *391*, 395.

[8] A. K. Smith in *Comprehensive Organometallic Chemistry II*, *Vol. 7* (Eds.: E. W. Abel, F. G. A. Stone, G. Wilkinson, D. F. Shriver, M. I. Bruce), Pergamon, Oxford, **1985**, p. 747.

[9] Z. Dawoodi, M. J. Mays, *J. Chem. Soc. Dalton Trans.* **1984**, 1931.

[10] R. C. Lin, Y. Chi, S. M. Peng, G. H. Lee, *J. Chem. Soc. Dalton Trans.* **1993**, 227.

[11] D. M. P. Mingos, A. S. May in *The Chemistry of Metal Cluster Complexes* (Eds.: D. F. Shriver, H. D. Kaesz, R. D. Adams), VCH, New York, **1990**, Chap. 2.

[12] The Ru–Ru distances in $[Ru_3(CO)_{12}]$ are in the range 2.8595–2.8515 Å: M. R. Churchill, F. J. Hollander, J. P. Hutchinson, *Inorg. Chem.* **1977**, *16*, 2655.

[13] With few exceptions, ^{1}H NOE enhancements are normally observed when the distance between the corresponding H atoms is shorter than 4 Å. See, for example: D. Neuhaus, M. Williamson, *The Nuclear Overhauser Effect in Structural and Conformational Analysis*, VCH, New York, **1989**, Chap. 3.

[14] J. D. Atwood, *Inorganic and Organometallic Reaction Mechanisms*, 2nd ed., Wiley-VCH, New York, **1997**.

[15] J. K. Shen, F. Basolo, P. Nombel, N. Lugan, G. Lavigne, *Inorg. Chem.* **1996**, *35*, 755.

[16] G. Lavigne, *Eur. J. Inorg. Chem.* **1999**, 917.

[17] a) J. A. Cabeza, F. J. Lahoz, A. Martín, *Organometallics* **1992**, *11*, 2754; b) N. Lugan, P. L. Fabre, D. de Montauzon, G. Lavigne, J. J. Bonnet, J. Y. Saillard, J. F. Halet, *Inorg. Chem.* **1994**, *33*, 434.

[18] A. A. Cherkas, N. J. Taylor, A. J. Carty, *J. Chem. Soc. Chem. Commun.* **1990**, 385.

[19] S. Parkin, B. Moezzi, H. Hope, *J. Appl. Crystallogr.* **1995**, *28*, 53.

[20] R. H. Blessing, *Acta Crystallogr. Sect. A* **1995**, *51*, 33.

[21] P. T. Beurskens, G. Beurskens, W. P. Bosman, R. de Gelder, S. García-Granda, O. R. Gould, R. Israël, J. M. M. Smits, The DIRDIF-96 program system, Crystallography Laboratory, University of Nijmegen, **1996**.

[22] G. M. Sheldrick, SHELXL97, version 97-2, University of Göttingen, Göttingen, **1997**.

[23] A. L. Spek, *The EUCLID Package in Computational Crystallography* (Ed.: D. Sayre), Clarendon Press, Oxford, UK, **1982**, p. 528.

[24] L. J. Farrugia, *J. Appl. Crystallogr.* **1999**, *32*, 837.

[25] Gaussian 98 (Revision A7), M. J. Frisch, G. W. Trucks, H. B. Schlegel, G. E. Scuseria, M. A. Robb, J. R. Cheeseman, V. G. Zakrzewski, J. A. Montgomery, E. Stratmann, J. C. Burant, S. Dapprich, J. M. Millam, A. D. Daniels, K. N. Kudin, M. C. Strain, O. Farkas, J. Tomasi, V. Barone, M. Cossi, R. Cammi, B. Mennucci, C. Pomelli, C. Adamo, S. Clifford, J. Ochterski, G. A. Petersson, P. Y. Ayala, Q.

Cui, K. Morokuma, D. K. Malick, A. D. Rabuk, K. Raghavachari, J. B. Foresman, J. Cioslowski, J. V. Ortiz, A. G. Baboul, B. B. Stefanov, G. Liu, A. Liashenko, P. Piskorz, I. Komaromi, R. Gomperts, R. L. Martin, D. J. Fox, T. Keith, M. A. Al-Laham, C. Y. Peng, A. Nanayakkara, C. González, M. Challacombe, P. M. W. Gill, B. Johnson, W. Chen, M. W. Wong, J. L. Andrés, M. Head-Gordon, E. S. Replogle, J. A. Pople, Gaussian Inc., Pittsburgh, PA, **1998**.

[26] A. D. Becke, *J. Chem. Phys.* **1993**, *98*, 5648.
[27] C. Lee, W. Yang, R. G. Parr, *Phys. Rev. B* **1988**, *37*, 785.
[28] P. J. Hay, W. R. Wadt, *J. Chem. Phys.* **1985**, *82*, 299.

Received: May 25, 2004
Revised: August 19, 2004
Published online: November 3, 2004

